# Estimating Coseismic Deformation of Southwestern Puerto Rico from the 7 January 2020 $M_{\rm w}$ 6.4 Earthquake: Constraints from Campaign and Continuous GPS

Alberto M. López-Venegas\*<sup>1</sup>, Glen S. Mattioli<sup>2,3,4</sup>, Margarita Solares-Colón<sup>5</sup>, David Mencin<sup>3</sup>, and Pamela E. Jansma<sup>4</sup>

#### **ABSTRACT**

The Puerto Rico-Virgin Islands (PRVI) block lies within the Northern Caribbean Plate Boundary Zone—a zone accommodating stresses between the larger North America and Caribbean plates. Data from Global Positioning System (GPS) sites throughout the PRVI block have been used to confirm the existence of a distinct microblock in the southwest. It is no coincidence that this portion of the PRVI block is the epicentral region of the 7 January 2020  $M_{\rm w}$  6.4 earthquake and the ensuing seismic sequence. Prior to the mainshock, the southwestern Puerto Rico (SWPR) region exhibited most of the onland seismic activity. The 2020-2021 SWPR earthquake seismic sequence has been characterized by having an atypical aftershock decay distribution occurring along multiple faults. As a result, fault parameters of the 7 January 2020 mainshock have been poorly defined by conventional seismic methods. Here, we present results from campaign and continuous GPS sites in SWPR, and compare GPS-derived displacements to those computed from the U.S. Geological Survey National Earthquake Information Center (NEIC) focal mechanism. We conclude that irrespective of which nodal plane is used, the observed coseismic displacements from GPS differ from those predicted using a simple elastic model and the NEIC focal mechanism. We infer based on these observations that the complex mainshock rupture resulted in a suboptimal double-couple solution.

#### **KEY POINTS**

- Global Positioning System (GPS) data from the SW PR
   7 January 2020 M<sub>w</sub> 6.4 are analyzed to evaluate coseismic deformation.
- GPS-derived displacements do not agree with predicted displacements from focal mechanism.
- Complex rupture of the earthquake reflects an immature deformation zone in the region.

# **INTRODUCTION**

The southwest Puerto Rico 7 January 2020  $M_{\rm w}$  6.4 event is the largest instrumentally recorded earthquake since the 11 October 1918  $M_{\rm w}$  7.2 (Doser *et al.*, 2005) earthquake, which impacted the northwest part of the island (López-Venegas, Hughes, and Vanacore, 2020; López-Venegas, Hughes, Vanacore, *et al.*, 2020). With a focal depth of 9 km and an epicenter only 13 km from the southern shore, the earthquake was felt islandwide and directly affected more than 500 houses, temporarily displaced more than 4000 residents, and required

more than \$240 million for recovery efforts from the Federal Emergency Management Agency. The seismic sequence started on 29 December 2019 with an  $M_{\rm w}$  5.0 earthquake and followed with several minor felt earthquakes until an  $M_{\rm w}$  5.8 event on 6 January 2020 occurred, serving as the main precursory event to the mainshock that struck the following day.

Two years after the onset of the seismic sequence, a total of 11 earthquakes with magnitudes larger than 5, and 95 events between  $M_{\rm w}$  4 and 5, were recorded by the Puerto Rico

1. University of Puerto Rico, Mayagüez, Puerto Rico, U.S.A., (a) https://orcid.org/0000-0002-3413-0546 (AML-V); 2. University of Texas, Arlington, Texas, U.S.A., (b) https://orcid.org/00000-0002-9117-7471 (GSM); 3. UNAVCO, Boulder, Colorado, U.S.A., (b) https://orcid.org/00000-0001-9984-6724 (DM); 4. University of Colorado-Denver, Denver, Colorado, U.S.A., (b) https://orcid.org/0000-0002-9051-8158 (PEJ); 5. University of Oregon, Eugene, Oregon, U.S.A., (b) https://orcid.org/0000-0002-9387-7551 (MS-C)

\*Corresponding author: alberto.lopez3@upr.edu

**Cite this article as** López-Venegas, A. M., G. S. Mattioli, M. Solares-Colón, D. Mencin, and P. E. Jansma (2022). Estimating Coseismic Deformation of Southwestern Puerto Rico from the 7 January 2020  $M_{\rm w}$  6.4 Earthquake: Constraints from Campaign and Continuous GPS, *Bull. Seismol. Soc. Am.* **113**, 99–114, doi: 10.1785/0120220115

© Seismological Society of America

Seismic Network (PRSN). Two years later, the PRSN located more than 18,000 aftershocks within the southwestern Puerto Rico (SWPR) region—a stark contrast of previous year's annual seismicity of 4000 events in the entire Puerto Rico-Virgin Islands (PRVI) block. The productivity of the sequence was atypical, producing more M > 4.5 magnitude aftershocks than average for an  $M_{\rm w}$  6 event (Liu et al., 2020). As a result, during the course of a few months after the mainshock, the U.S. Geological Survey (USGS) aftershock forecast team required several modifications to the model to adjust the unusually high-observed production. Another interesting observation is the poor double-couple percentage of the mainshock of the published USGS moment tensor (52%), which has led other researchers to infer complex, multiple-fault rupture dynamics for this event. Within five months of the mainshock, earthquake relocations helped reveal a quasi-parallel, criss-cross pattern of faults trending northwest-southeast and northeast-southwestan evidence that is in agreement with either pure strike slip, or normal focal mechanisms from the USGS, Global Centroid Moment Tensor and/or PRSN moment tensor computations. In this study, we present results from Global Positioning System (GPS) sites in southwest Puerto Rico, including two decades of GPS observations from campaign and continuous sites, and one year of postseismic continuous observations in the epicentral and aftershock region, which were obtained from an National Science Foundation Rapid Response Research (NSF RAPID) deployment of six new continuous GPS (cGPS) stations. We compute static coseismic displacements using Okada dislocations within an elastic half-space and compare them to observed values from our composite GPS network.

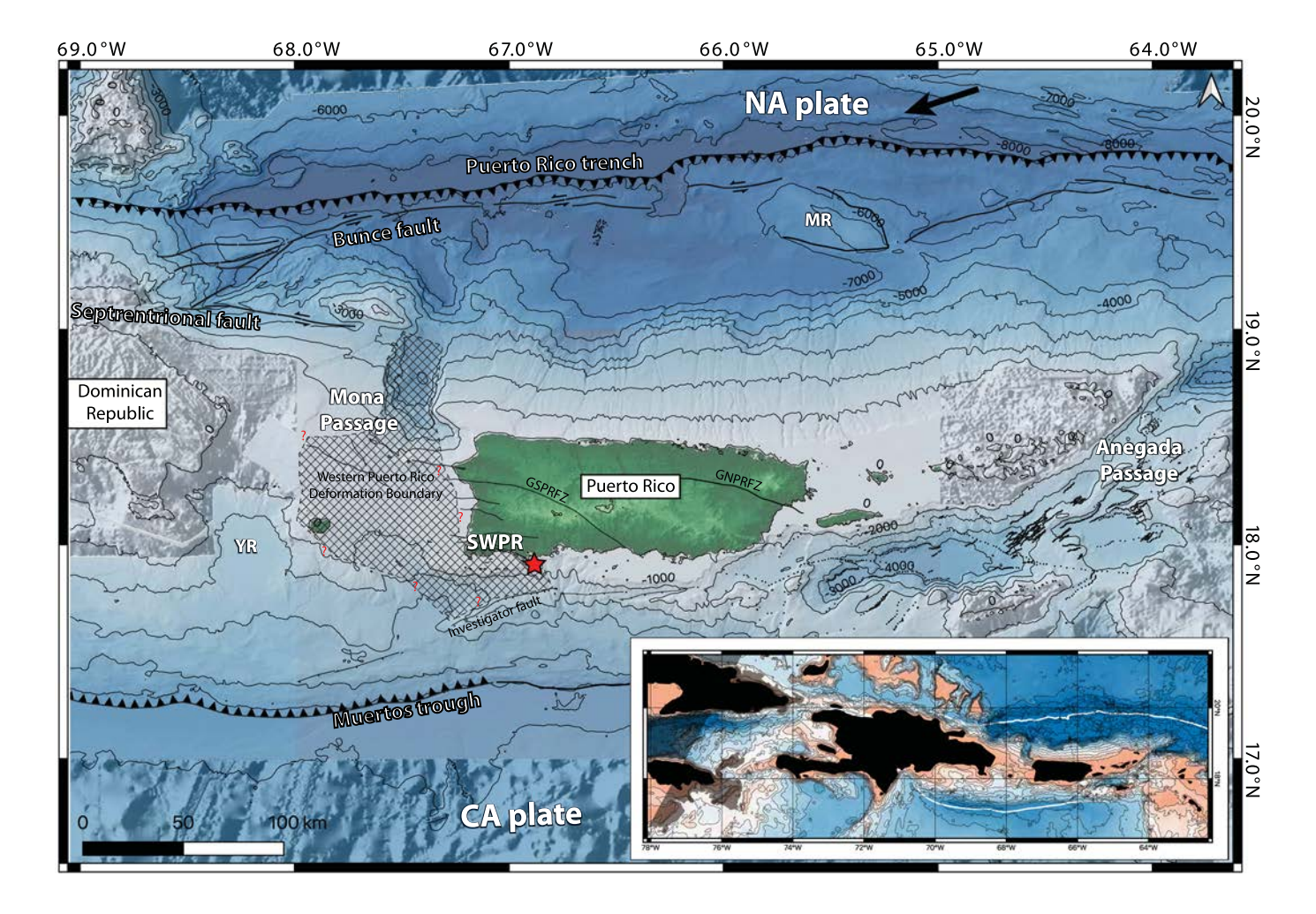
# THE PRVI MICROBLOCK AND SOUTHWESTERN PRVI SEGMENTATION

The 7 January 2020  $M_{\rm w}$  6.4 earthquake occurred near the southern boundary of the PRVI block. PRVI is one of at least four tectonic blocks within the Northern Caribbean Plate Boundary Zone (NCPBZ; Mann and Burke, 1984; Masson and Scanlon, 1991; Jansma et al., 2000; Benford et al., 2012) that accommodates strain due to the highly oblique contraction between the North America (NA) plate and the Caribbean (CA) plate (Jansma et al., 2000; Jansma and Mattioli, 2005). Figure 1 shows the location of Puerto Rico with prominent tectonic and geologic features that relate to the 2020 SWPR seismic sequence. To the north, the PRVI block interacts with the NA plate at the Puerto Rico trench, whereas a retroarc wedge to the south, along the Muertos trough, marks the boundary with the Caribbean crust (ten Brink et al., 2009; Granja Bruña et al., 2015). Although both northern and southern PRVI boundaries exhibit typical oblique subduction-related tectonic boundary features, the eastern (Anegada Passage) and western (Mona Passage) boundaries show more complex structures that may reflect young crustal deformation transitioning from one regime to another (Chaytor and ten Brink, 2010; Laurencin et al., 2017).

Knowing where the motion is accommodated throughout the western PRVI boundary along the Mona Passage is challenging, because there is no single geologic feature connecting the Puerto Rico trench to the north, to the Muertos trough to the south. The most evident block boundary is the Mona rift—a predominantly north-south-trending normal-faulting feature that Jansma and Mattioli (2005) concluded allowed a few millimeters per year of extension. As a result, kinematics of this region remain elusive, because the Mona rift can account for only a fraction of the entire deformation between PRVI and Hispaniola. Though the Mona rift is interacting with the Septentrional and Bunce faults to the north along the fore-arc, the Mona Canyon, the resulting feature from the rifting increasingly becomes shallower southward as it reaches the Desecheo ridge. How the deformation is accommodated farther south to the Muertos trough is unclear, and it is also questionable whether it goes inland through SWPR, or if it continues south and connects to the Yuma rift and the Muertos trough, hence the western PR deformation boundary (Fig. 1) (Chaytor and ten Brink, 2010; ten Brink et al., 2022). Owing to the seismic activity of the southwest, it is possible that the seismic sequence discussed here is the product of these complex interactions.

Deciphering the current kinematics of the Mona Passage is complicated because rifting is only observed partially, in this case at the Mona rift, because it does not extend through the entire deformation area, that is, from the Puerto Rico trench to the Muertos trough. This poses an intriguing situation, because other geologic features must exist that accommodate motion apart from the Mona rift, and these are still largely unknown. Chaytor and ten Brink (2010) demonstrated the existence of oblique-extensional features trending-west and north-northwestern within the Oligocene-Pliocene strata within the central portion of the Mona Passage, but they were unable to estimate amount and timing of extension in the region. Moreover, crustal deformation assessment from their bathymetric mapping and seismic reflection data seems to suggest that the southern half of the Mayagüez basin is either not affected, or features are buried, or we are currently under a transitioning state where stresses have not yet reached the area. In any case, how the deformation observed at the Mona Rift connects to the Muertos trough to the south is poorly understood. Recent GPS observations, which may help shed light into the matter, have demonstrated the existence of a separate SWPR microblock (Jansma and Mattioli, 2005; López et al., 2011; Solares-Colón, 2019).

GPS data from the PRVI block have been used for the past two decades to estimate its motion with respect to NA (Dixon et al., 1998), understand its role within the NCPBZ and motion with respect to the CA plate (Jansma et al., 2000; Jansma and Mattioli, 2005), and quantify internal deformation (López et al., 2011; Solares-Colón, 2019) to confirm the existence of a separate SWPR block. Solares-Colón (2019) performed simple baseline



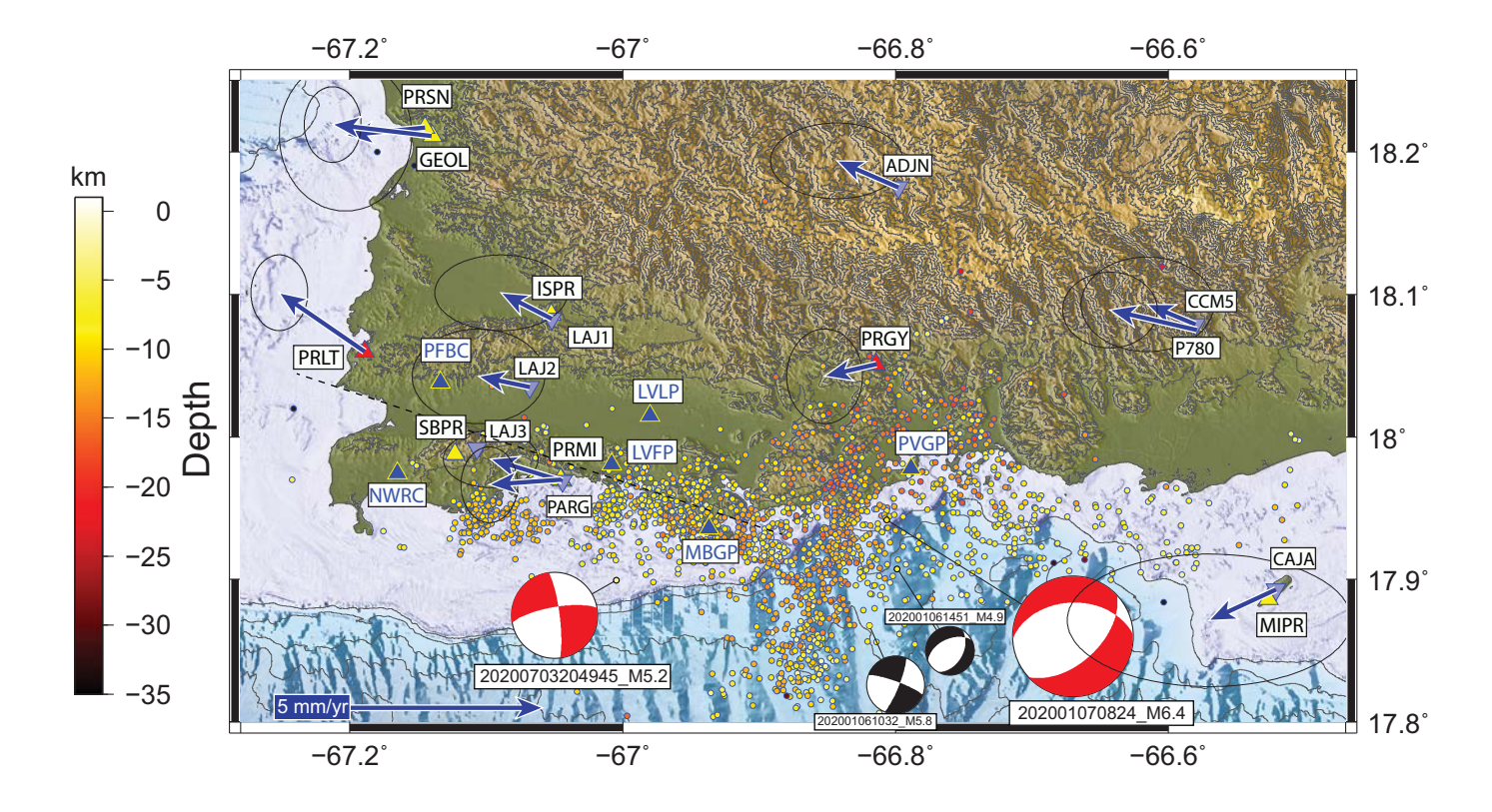
computations among GPS sites within the PRVI block and eastern Hispaniola, and inverted GPS residuals to obtain an angular velocity vector for the PRVI and SWPR block pair. Although the current GPS network was able to confirm the SWPR block, a more dense network in SWPR is necessary to help identify the location of active faults accommodating associated deformation and relative motion between PRVI, SWPR, and the CA plate. Installation of the six new cGPS sites in southwestern PR in 2021 help densify the region with sensors that would allow a better definition of the SWPR block and how it relates to the Mona Passage. However, similar to other Caribbean islands GPS studies, sites onland are only able to resolve to a certain extent and thus are limited in their capability.

Regardless of the crustal deformation pattern that has evolved in the region that separates the PRVI block from Hispaniola, the important fact remains that the predominant northeast–southwest compression direction of the northeastern Caribbean in combination with the heterogenous composition of the arc have led to the development of multiple faults throughout the Mona Passage that still have yet to reach maturity (ten Brink *et al.*, 2022). Understanding the coupling of the NA subducting slab underneath the PRVI block is critical to develop models seeking to explain the deformation zone at the Mona Passage.

**Figure 1.** Shaded relief map of the Puerto Rico—Virgin Islands (PRVI) block with tectonic boundaries and main geological features. Red star denotes 7 January 2020 mainshock epicenter. Lower right inset shows the Northern Caribbean Plate Boundary Zone with Greater Antilles Islands in black. Solid black arrow represents the North America-Caribbean convergence direction of 19 mm/yr. Hashed polygon represents the western Puerto Rico (PR) Deformation Boundary within the Mona Passage—the boundary between PRVI and Dominican Republic to the west. YR and MR are the Yuma rift and Main ridge, respectively.

## THE 2020 SWPR EARTHQUAKE SEQUENCE

Seismic activity in the epicentral region began on 28 December 2019 with an *M* 4.7 earthquake, followed by an *M* 5.0 the day after just 5 km west of where the mainshock epicenter would occur later. These two events, and all those that followed until 6 January 2020, were characterized by nearly pure strike-slip fault ruptures, either on a northeast–southwest left-lateral fault or on an orthogonal right-lateral system trending-northwest–southeast. At the start of the sequence, PRSN scientists attributed this set of events to an offshore extension of the Punta Montalva fault (PMF; Addarich-Martínez, 2009)—a left-lateral, north-northwest–south-southeast-trending fault that has been postulated to merge with the North Boquerón Bay (NBB) fault farther west (Roig-Silva *et al.*, 2013). Although these two faults have been



suggested to accommodate motion along the Lajas Valley (see Fig. 1), geophysical and paleoseismic evidence is still necessary to confirm their primary role in southwestern PR. Whether faults of the Lajas Valley are directly related to the faults of the January 2020 seismic sequence is still a matter of debate.

Two seismic events on 6 January 2020 marked the turning point of events (refer to focal mechanisms with black compressional quadrants in Fig. 2); at 10:32:18 UTC, an *M* 5.8 occurred with the same prevalent characteristic strike-slip mechanism, but four hours later, an *M* 4.9 event produced a normal-fault mechanism that likely unclamped the fault that led to the rupture of the mainshock that followed the next day on 7 January. Interestingly, the USGS-computed moment tensor for the *M* 4.9 event occurring at 14:51:17 UTC has a 100% double-couple (DC) and a strikingly similar focal mechanism to that of the mainshock.

Events following the mainshock produced either normal or strike-slip focal mechanisms with predominant northeast-southwest strikes. This generated confusion among PRSN scientists in charge of the interpretation of the rupture process and assessment of the evolving seismic hazard. How the seismic activity progressed offshore brought concerns of possible stress transfers into the PMF or even toward NBB. Although some events did occur inland along these two faults (mainly PMF and related minor fault strands), most of the activity was concentrated offshore near the epicentral region, with both types of the predominant focal mechanisms (strike slip and normal) occurring along the reactivation of faults. Some of these faults have been mapped, but others have yet to be properly identified. A USGS-funded project to update the Puerto

**Figure 2.** Map showing premainshock Global Positioning System (GPS)-derived velocity field, focal mechanisms of the 7 January 2020 mainshock (right) and 3 July 2020 aftershock (left) in red, focal mechanisms (black) of precursory events occurring on 6 January 2020, and aftershocks  $M_{\rm w} > 3$  colored by focal depth. Also shown are GPS sites used in this study: Triangles are continuous GPS (cGPS) sites, and inverted triangles are episodic GPS (eGPS) sites. Puerto Rico Seismic Network (PRSN) sites are colored yellow, HLCM are red, and dark blue are postearthquake permanent installations. Black dashed line is the trace of the suggested North Boquerón Bay—Punta Montalva fault, as suggested by Roig-Silva *et al.* (2013).

Rico Seismic Hazard Map is expected to yield valuable fault information in the region.

#### The 7 January 2020 mainshock

The 7 January 2020  $M_{\rm w}$  6.4 southwestern Puerto Rico earth-quake occurred at 08:24:25 UTC, at a shallow depth (7–9 km) on a normal fault beneath the Guayanilla Canyon. Some inconsistencies in the data products for the event suggest a complex rupture process. Two hypocenters have been reported (The PRSN location lies ~5 km from the coast, whereas the USGS lies 10 km farther south), and the best moment tensor solution published by the USGS yields a 52% DC. The fact that three precursor events occurring the day before the  $M_{\rm w}$  6.4 event showed consistent normal focal mechanisms, however, suggests that the mainshock also may have occurred on a normal fault, despite the poor DC reported for the USGS focal mechanism. Identifying the fault plane that ruptured on the day of the event has proven difficult; it was either an east-

northeast-west-southwest northward steeply dipping fault plane or a shallow fault plane dipping toward the SE.

Within days of the sequence, it was evident from the after-shock distribution that motion must have taken place along several antithetic faults. Subsequent seismic data analysis confirmed a complex rupture (Liu *et al.*, 2020), which is thought to be the result of a young, active, and unstable deformation zone (ten Brink *et al.*, 2022).

The USGS focal mechanism has fault parameters 268, 43°, -58° for nodal plane 1 (henceforth named MNP1), and 47°, 54°, -116° for nodal plane 2 (henceforth MNP2). For each nodal plane, we used Okada dislocations within an elastic half-space to estimate static displacements at GPS sites.

#### **Aftershocks**

More than 18,000 aftershocks (M > 3.0) have been located by the PRSN within the epicentral region (Figs. 1, 2). The aftershock distribution suggests interaction of multiple faults. At least three distinctive faults have been identified; two of them show northwest-southeast trends and one that is roughly orthogonal, trending-northeast-southwest. Aftershock distribution follows the average nodal plane orientation of M > 4.5 focal mechanisms computed by the National Earthquake Information Center (NEIC). Owing to the unusual seismic activity production, aftershock analysis during the sequence required moving from the USGS-automated Reasenberg and Jones (1989) model to the epidemic-type aftershock sequence model (van der Elst et al., 2022) that allows for significant aftershocks in the sequence to trigger their own aftershocks. The lack of agreement of the sequence with Båth's law and the lower-than-expected mainshock energy release estimate have been credited for the atypical seismic sequence (ten Brink et al., 2022).

# The 3 July 2020 aftershock

The 3 July 2020  $M_{\rm w}$  5.3 earthquake was one of the most significant aftershocks in the sequence. With a focal depth of 8 km and epicenter just 7 km south of the trace of PMF, this aftershock had intensity of modified Mercalli intensity (MMI) VI and was widely felt throughout the island. What makes this aftershock interesting is the prominent coseismic displacement in nearby cGPS sites PRMI and PRGY at 9 and 27 km epicentral distance, respectively. Owing to the proximity of the earthquake to station PRMI, the observed coseismic displacement in the cGPS horizontal components time series is larger than that observed for the 7 January 2020 mainshock. The USGS focal mechanism for this event yields a steeply northward-dipping east-west-trending left-lateral strike fault or an orthogonal nodal plane that trends roughly north-south and dips eastward (Fig. 2). None of these options fit particularly well with the overall principal stress direction obtained from the previous moment tensors in the region. Taking into consideration the observed left-lateral fault system in the region, however, the nodal plane: 260°, 75°, -10° (henceforth ANP1) may be

the rupture plane and the other nodal plane (henceforth ANP2): 353°, 80°, -165° the auxiliary plane.

#### THE SOUTHWESTERN PR GPS-GNSS NETWORK

More than two dozen cGPS sites operated by multiple agencies exist in Puerto Rico. Whether privately owned by surveying companies, or from state or federal agencies, these sites provide data that is accessible, open, and freely available. PRSN alone maintains 20 cGPS sites throughout the island. Private survey company HLCM Group operates and maintains a total of seven cGPS sites within PR, and are part of National Oceanic and Atmospheric Administration (NOAA) National Geodetic Survey (NGS) Continuous Operating Reference Station (CORS). The PRVI episodic GPS (eGPS) network consists of 15 sites distributed across PVRI. The first two sites from the eGPS network were installed during the 80's and later augmented during the following decade. For this study, we concentrate on sites of southwestern PR (Fig. 2, Table 1), where a displacement in the time series was observed during the earthquakes of 7 January and 3 July 2020. Sites farther away from the epicentral region were not included in our analysis of the coseismic displacement, because the estimated offsets in the time series were insignificant, that is, within the daily root mean square for the position estimates.

#### Continuous sites

A total of six cGPS sites in southwestern PR are located within the footprint of the affected area of the mainshock. Of these, only five were operating when the earthquake occurred (PRGY, PRLT, PRMI, P780, and SBPR). Table 1 shows these sites with their location and time span. Two of the six sites belong to HLCM Group and are part of the NOAA/NGS CORS program (PRGY, and PRLT), and two sites belong to the Puerto Rico Seismic Network (MIPR, and SBPR). Site SBPR was installed in November 2019 and was recording for two months when the mainshock occurred. In contrast, site MIPR in Caja de Muerto Island went offline after Hurricane Maria struck in September 2017. Access and logistics to the island were challenging but PRSN was able to bring the site back online in early 2021. The last two sites, PRMI, and P780 belong to NOAA-NGS, and UNAVCO, respectively.

#### Campaign sites

The Geodesy Lab at the Department of Geology—University of Puerto Rico at Mayagüez often reoccupies sites from the Puerto Rico campaign or eGPS network. A total of eight eGPS sites of western Puerto Rico were remeasured immediately after the mainshock. These sites are ADJN (Adjuntas), CAJA (Caja de Muerto Island), LAJ1, LAJ2, and LAJ3 (spanning the Lajas Valley), PARG (Lajas), and SALN (Salinas), and are also shown in Table 1 with their location and time span. Unfortunately, none of these sites have data during the year prior to the mainshock, thus estimating a reliable coseismic displacement was not

TABLE 1
Location, Velocities (IGS14 and Caribbean Fixed), Time Span, and Number of Observations of GPS Sites Used in This Study

					IGS 2014 (mm/yr)					CA-Fixed Velocity (mm/yr)							
Site ID	Latitude (°N)	Longitude (°E)	HAE (m)	V <sub>N</sub>	$\sigma_{V_N}$	V <sub>E</sub>	$\sigma_{V_E}$	v <sub>v</sub>	$\sigma_{V_V}$	V <sub>N</sub>	$\sigma_{V_N}$	V <sub>E</sub>	$\sigma_{V_E}$	v <sub>v</sub>	$\sigma_{V_V}$	Time Span (yr)	Number of Observations
ADJN	18.175	293.202	520.576	13.5	0.3	8.9	0.5	-2.9	0.8	0.69	0.3	-1.59	0.5	-2.9	0.8	20.4973	55
CAJA	17.893	293.479	35.048	12.1	0.4	8.9	0.7	3.6	1	-0.8	0.4	-1.73	0.7	3.6	1	18.0079	15
CCM5	18.079	293.420	155.513	13.4	0.3	9.3	0.6	-1.6	0.9	0.52	0.3	-1.25	0.6	-1.6	0.9	20.7842	40
LAJ1	18.083	292.948	20.737	13.4	0.3	9.2	0.5	-3.2	0.8	0.67	0.3	-1.31	0.5	-3.2	8.0	20.3415	63
LAJ2	18.035	292.932	-5.614	13.0	0.3	9.2	0.5	-1.6	0.7	0.28	0.3	-1.33	0.5	-1.6	0.7	20.3415	93
LAJ3	17.992	292.893	181.523	11.5	0.4	10.9	0.6	-0.1	0.9	-1.21	0.4	0.35	0.6	-0.1	0.9	20.694	22
LVFP	17.981	292.992	-19.394	10.0	1.4	7	1.1	-8.4	2.4	-2.74	1.4	-3.56	1.1	-8.4	2.4	1.1726	423
LVLP	18.015	293.020	-35.4626	15.9	1.5	7.9	1.3	2	2.7	3.15	1.5	-2.65	1.3	2	2.7	0.9151	335
MBGP	17.936	293.063	5.4641	5.7	1.7	9.9	1.1	-16.3	2.6	-7.07	1.7	-0.68	1.1	-16.3	2.6	1.1534	416
MIPR	17.886	293.473	-38.1224	13.5	0.4	9.1	0.4	-0.7	0.7	0.6	0.4	-1.53	0.4	-0.7	0.7	8.9544	2391
NWRC	17.975	292.835	-14.9779	14.9	4.4	7.6	8.5	0.9	12.8	2.21	4.4	-2.95	8.5	0.9	12.8	0.6685	245
P780	18.075	293.421	154.07	14.0	0.4	8.8	0.3	0	0.6	1.12	0.4	-1.75	0.3	0	0.6	11.5956	4177
PARG	17.969	292.956	-12.315	13.6	0.3	8.8	0.4	-0.1	0.6	0.87	0.3	-1.76	0.4	-0.1	0.6	27.3836	96
PFBP	18.038	292.867	3.661	15.4	1.2	8.2	1.2	0.4	2.6	2.7	1.2	-2.33	1.2	0.4	2.6	1.1123	367
PRGY	18.051	293.186	33.8814	12.5	0.5	9.2	0.4	-2.7	8.0	-0.31	0.5	-1.34	0.4	-2.7	8.0	9.7342	3308
PRJC	18.342	293.001	22.8497	13.5	0.4	8.9	0.4	-0.6	0.7	0.76	0.4	-1.51	0.4	-0.6	0.7	9.737	3393
PRLT	18.060	292.811	-15.2397	14.2	0.4	8.3	0.3	-0.8	0.7	1.52	0.4	-2.21	0.3	-0.8	0.7	9.5836	3376
PRMI	17.970	292.955	-25.477	12.6	0.4	8.7	0.3	-0.3	0.5	-0.13	0.4	-1.86	0.3	-0.3	0.5	13.7671	4636
PRN4	18.079	293.631	129.1832	13.5	0.4	9	0.4	0.5	8.0	0.55	0.4	-1.56	0.4	0.5	8.0	9.9123	3422
PRSN	18.217	292.855	-14.8337	12.5	8.0	8.4	0.7	2.8	1.8	-0.2	8.0	-2.05	0.7	2.8	1.8	4.4301	1339
PVGP	17.978	293.212	-2.3774	13.0	1.3	6.5	1.4	-1.4	2.6	0.19	1.3	-4.08	1.4	-1.4	2.6	0.9616	346
SALN	18.029	293.766	130.467	14.2	0.5	8.8	0.7	1.2	1.1	1.2	0.5	-1.79	0.7	1.2	1.1	15.0528	30
SBPR	17.988	292.877	168.9942	15.5	1	5.5	1	-4.8	3.4	2.8	1	-5.05	1	-4.8	3.4	2.2877	767

Bold fonts denote continuous GPS (cGPS) sites, otherwise the site is an episodic site (eGPS). ADJN, Adjuntas; CAJA, Caja de Muerto Island; and PRSN, Puerto Rico Seismic Network.

possible. Of these, only one site (LAJ3) was remeasured, but the data was unusable.

#### **NSF RAPID sites**

Following the 7 January 2020 mainshock, the PRSN presented a RAPID proposal to NSF with the objective of adding geodetic instrumentation to the region. As a result, PRSN received funds to install six new sites with the capability of tracking and recording both GPS and GLONASS satellites. These Global Navigation Satellite System (GNSS) sites are located within the footprint of onland southwestern PR faults (blue triangles in Fig. 2). These sites, installed between late 2020 and early 2021 (in order; LVFP, PFBC, MBGP, PVGP, LVLP, and NWRC), consist of stainless steel short-drilled braced monuments and provide real-time data through commercial cellular infrastructure. For this study, the longest processing time span of these sites is 1.1726 yr for LVFP, and the shortest processing time span of these sites is 0.6685 yr for NWRC.

#### **DATA AND ANALYSIS**

# Acquisition and repositories

GPS data collection in the northeastern Caribbean began in 1986 at seven locations (Dixon *et al.*, 1998), and these stations

were reoccupied in 1994 and 1995. Additional stations in PR and the US and British Virgin Islands were installed in 1994 and 1995 (Jansma et al., 2000), and reoccupied at various intervals throughout the late 1990s through the 2010s. The details of these early campaign or eGPS observations may be found in the original papers, and two master's theses (López et al., 2011; Ihemedu, 2012; Solares-Colón, 2019) provide additional details related to the later occupations of these campaign sites, including the antenna-receiver combinations used to collect the raw GPS observations. All eGPS data collected and used for the previously published and current analysis was GPSonly, dual-frequency (L1/L2) code and phase observations. Only daily observations that had at least 6 hr of continuous arc were included in the final kinematic analysis. Hatanakacompressed GPS (RINEX 2.11) data from continuous stations were acquired from two primary archives, including UNAVCO and the NGS CORS network. In addition, campaign data from stations established initially in the 1990s (Dixon et al., 1998; Jansma et al., 2000; Jansma and Mattioli, 2005) and reoccupied before and after the 7 January 2020 mainshock were also provided directly by the PRSN. Metadata were also obtained from the data repositories from which the RINEX data were obtained.

Daily (24 hr) Hatanaka-compressed RINEX files were converted to RINEX (v.2.11) observation files and renamed for processing. As part of a larger reprocessing effort to update and refine the PRVI block interseismic velocity field (Jansma et al., 2000; Jansma and Mattioli, 2005; López et al., 2011; Ihemedu, 2012; Solares-Colón, 2019), data from a total of 68 stations, including 23 campaign or eGPS sites and 45 cGPS stations, were obtained and prepared for processing and kinematic analysis. GPS L1/L2 code phase data from cGPS stations were processed through 31 March 2022, and eGPS sites were processed through the last available epoch. Six new cGPS stations were established in southwestern PR with NSF-RAPID funding provided to UPRM after the 7 January 2020 mainshock (PI López). One proximal and newly established cGPS station, SBPR, located in the El Conuco National Protected Area, Sierra Bermeja, Puerto Rico, and installed in late 2019 was operating at the time of the M 6.4 mainshock. The six other NSF-funded cGPS stations were installed in 2021 and therefore are only useful to examine postseismic deformation. Table 1 has details related to the number of daily (24 hr) observations and length of the time series included in the analysis.

## **Processing and analysis**

RINEX (v.2.11) data were processed with the National Aeronautics and Space Administration Jet Propulsion Laboratory (JPL) software suite GIPSY-OASISII (v.6.4) using an nonfiducial, absolute point positioning strategy (Lichten, 1990; Heflin et al., 1992; Zumberge et al., 1997) through gd2p and other executable codes embedded in various scripts for ease of processing and analysis. Final, nonfiducial orbit, clock, and Earth orientation (OEP) products (Repro3-IGS14) Lichten and Border (1987) were obtained from the JPL along with nonfiducial wide-lane phase bias files and so called "xfiles," which were used to translate, rotate, and scale the loosely constrained, daily-satellite-frame or "free-network" ambiguity-resolved, absolute point positions into the JPL realization of IGS14 (Altamimi et al., 2016). Ocean loading coefficients (Scherneck, 1991), corrected for both ocean and solid earth motion and using the FES2004 global gravity model, were obtained from the Onsala Space Observatory to align with the models used by JPL for their OEP products. Tropospheric delays were estimated using standard VMF1 2.5 × 2 grid (Boehm et al., 2006) files from the Technical University of Vienna. All our GOA-II processing used absolute antenna phase center models from the JPL-provided igs14\_2163.atx ANTEX file, and processing assumed elevation cutoff of 7° above the horizon.

Examples from a long-running cGPS station, BYSP, located in Bayamón, Puerto Rico, far from the 7 January 2020 *M* 6.4 earthquake, and a campaign station established in 1986 with its first useful GPS data in 1994, ISAB, are shown relative to IGS14 and CA-fixed frames in Figures 3 and 4, respectively. Linear velocities were estimated along with estimates of the NEV-

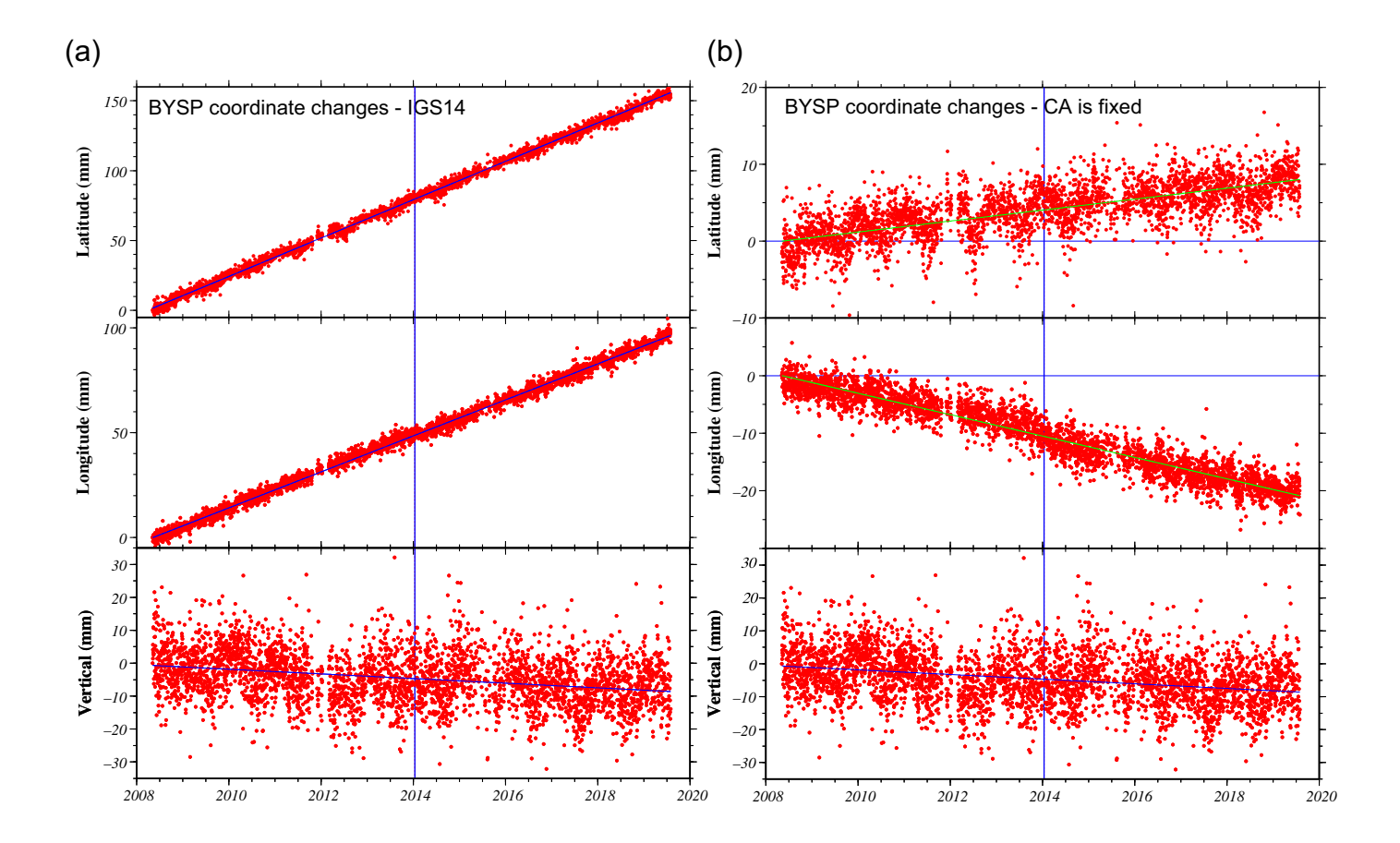
component white and flicker noise (Mao et al., 1999), and 1 mm/sqrt (yr) of random walk monument noise was assumed. IGS14 position estimates were placed into a Caribbean-fixed frame using an Euler pole (DeMets et al., 2000, 2007) defined by a global analysis of GPS and other kinematic data (DeMets et al., 2010) and updated into IGS14 (C. DeMets and G. Mattioli, personal comm., 2021). The Euler pole location and rotation rate for CAR with respect to ITRF14 we applied is -37.013° N, 79.240° E, 0.2583°m.y. (counter-clockwise). In rare cases, offsets that are unrelated to known geophysical events or were not fully removed due to known equipment changes (e.g., antenna-model changes or changes in antenna height) were calculated to remove offsets in the time series. Methods to estimate these offsets are discussed further subsequently. Details of the station component velocities in IGS14, noise estimates, correlation of horizontal components, length of observation, and CAR-fixed velocities are in Table 1.

GOA-II processing using gd2p yielded both nonambiguityresolved and ambiguity-resolved, daily "free-frame" position estimates and covariances. These initial position estimates were translated, rotated, and scaled using apply and JPL-provided xfiles into IGS14. Only ambiguity-resolved, IGS14 position estimates and their covariances were used for any further geodetic analysis. Time series were produced, analyzed, and plotted using SuperVel (written by C. DeMets and modified by G. Mattioli), Generic Mapping Tools (GMT; Wessel and Smith, 1998), and other user-written scripts. For stations considered in this analysis, the initial inversion of the position estimates for NEV-component velocities and errors was iterated to remove residual NEV outliers of 20, 30, and 40 mm ( $\sim$ 4 $\sigma$ for each component), respectively, and then the initial position, linear velocities, and errors were re-estimated. For most cGPS time-series examined here, the reduced Chi-squared was less than 1 mm in each NEV-component.

#### **COSEISMIC DISPLACEMENT ESTIMATES**

As discussed earlier and shown in Figures 3 and 4, time series based on ambiguity-resolved, absolute point positions, and covariances from GOA-II were postprocessed using SuperVel to calculate NEV-component linear velocities and errors, including estimates of white, flicker, and random walk noise in either the IGS14 and CAR-fixed frames. SuperVel can calculate two types of offsets in positional time series: (1) constant velocity offset at any specified, but arbitrary epoch within the data window; and (2) a five-day offset at a specified epoch, which is done prior to the linear inversion to obtain the NEV-component velocity and noise estimates. This method averages five days of position estimates before and after the specified epoch and simply calculates the difference in the average NEV positions. In addition, SuperVel allows the user to time window the data to a specified epoch before calculating velocities and offsets.

In the event of a geophysical event, such as an earthquake that results in measurable coseismic displacement at any



arbitrary station, method (2) above is the preferred method to estimate that offset. This, of course, requires that continuous, daily, observations are available for periods before and after the epoch of the earthquake. This method does introduce a small bias into a coseismic displacement estimate, because position estimates for days immediately after the earthquake may also include some afterslip. For large events (M > 7) proximal to any cGPS station, this bias is on the order of several millimeters to a couple of centimeters; given that the coseismic displacement is usually an order of magnitude larger than this potential bias in the five-day offset estimate, five-day offsets discussed subsequently should be considered the maximum coseismic displacements, as they may contain some additional displacement that should be considered afterslip. Once such an offset has been estimated, continued afterslip is often clearly observable in the cGPS time series. Modeling of the afterslip may be used to correct the bias in the initial coseismic displacement estimate, but the coseismic offsets reported in Table 2 are the initial, uncorrected estimates. An example in which method (2) was applied at cGPS station PRLT in Cabo Rojo, Puerto Rico, is shown in Figure 5.

Method (1) above may be applied when GPS observations are available for some period (i.e., interseismic) before the earthquake and again after the event. Here, we apply the constraint that the NEV-component velocities are constant and linear, and the offset is adjusted at the epoch of the event as part of the inversion to constrain the linear velocity and noise estimates. This method has been applied to eGPS stations

**Figure 3.** Time series for cGPS station BYSP in Bayamón, Puerto Rico. (a) Results in IGS14 with the blue lines showing linear fits to the position estimates and (b) results in a CA-fixed frame with the green lines showing the fit relative to the fixed CA plate. Each red dot represents a 24 hr position estimate. The vertical blue line in both the panels denotes the 13 January 2014  $M_{\rm w}$  6.4 earthquake and the epoch at which a five-day offset was calculated (see the Coseismic displacement estimates section). The color version of this figure is available only in the electronic edition.

that have long interseismic observation epochs prior to the  $M_{\rm w}$  6.4 mainshock and other regional earthquakes, and reoccupations to obtain data recently after the event. Again, because the postseismic observations are usually not available immediately after the earthquake of interest, they may also be biased with some amount of afterslip. An example in which method (1) was applied at eGPS station LAJ1 in Cabo Rojo, Puerto Rico, is shown in Figure 6.

# The 7 January 2020 mainshock

As indicated earlier, we employed the USGS-derived focal mechanism to compute the static displacement at each of the sites where a displacement was observed in the GPS time series. Because of the complex rupture observed, we computed displacement using both nodal planes (MNP1 and MNP2) and compared those to the observed data (Figs. 7 and 8). Our results indicate that neither of the nodal planes' predicted displacements resemble the observed pattern of deformation (Table 2). This is

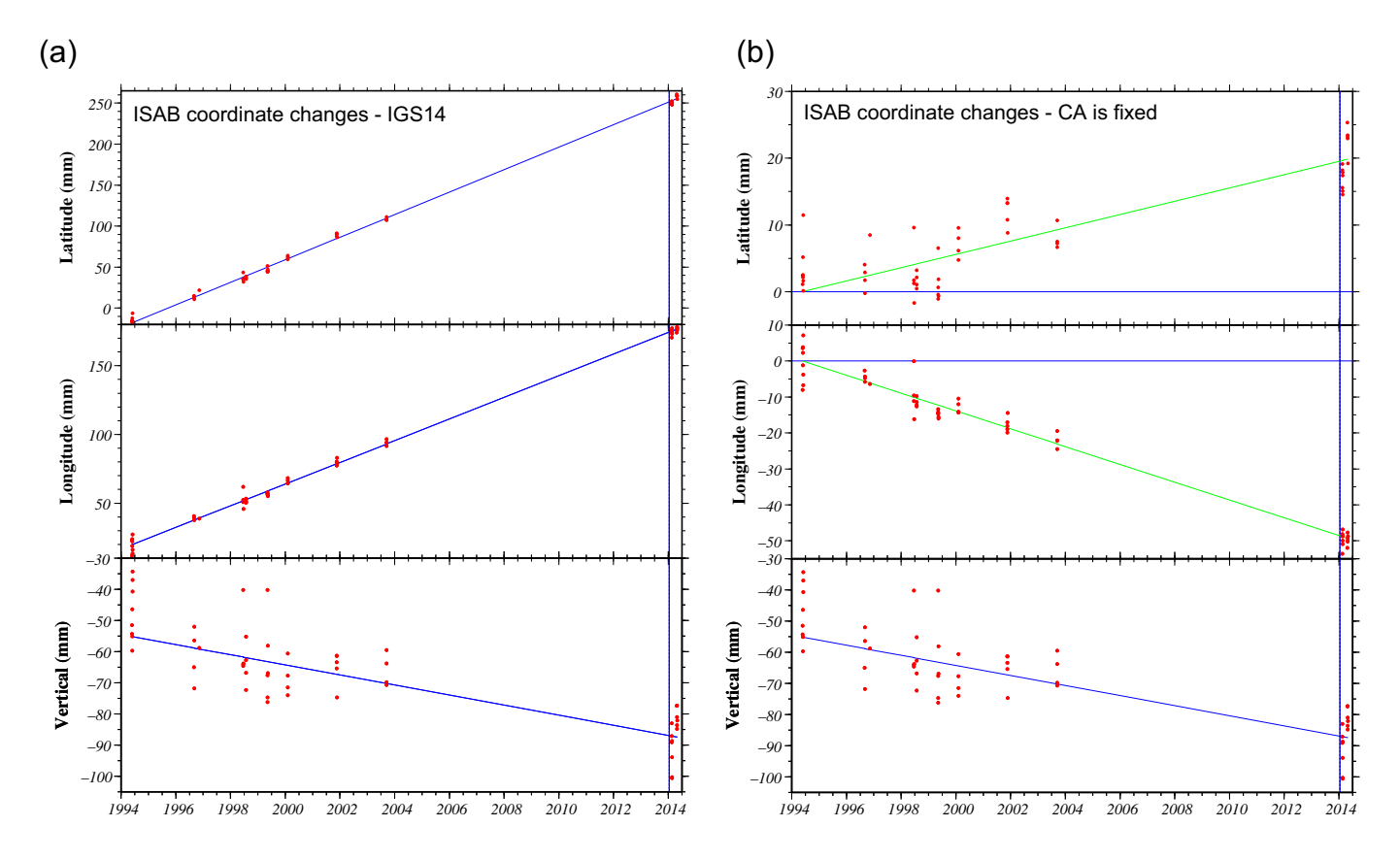


**Figure 4.** Time series for eGPS site, ISAB, established in 1986, but with the first useful GPS data in 1994. (a) Results in IGS14 with the blue lines showing linear fits to the position estimates and (b) results in a CA-fixed frame with the green lines showing the fit relative to the fixed CA plate. Each red dot represents a 24 hr position estimate. The vertical blue line in

both the panels denotes the 13 January 2014  $M_{\rm w}$  6.4 earthquake and the epoch at which a constant velocity offset was calculated (see the Coseismic displacement estimates section). The color version of this figure is available only in the electronic edition.

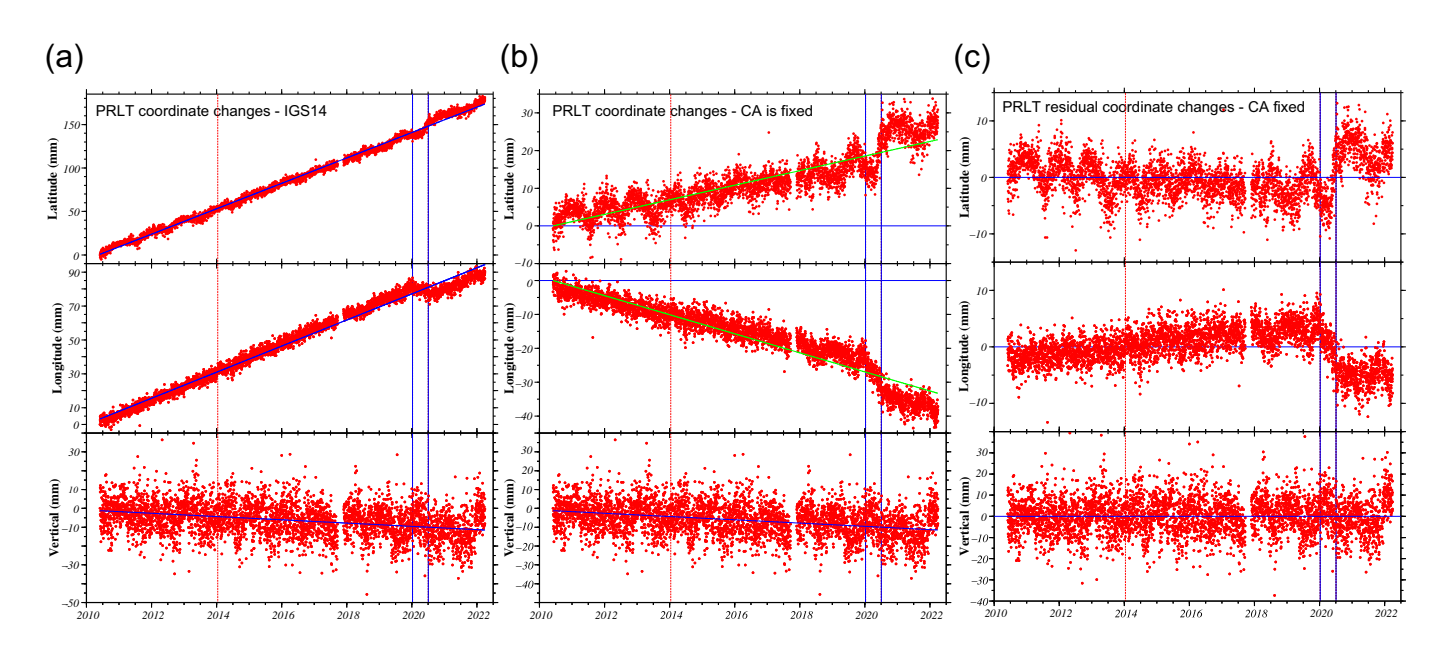
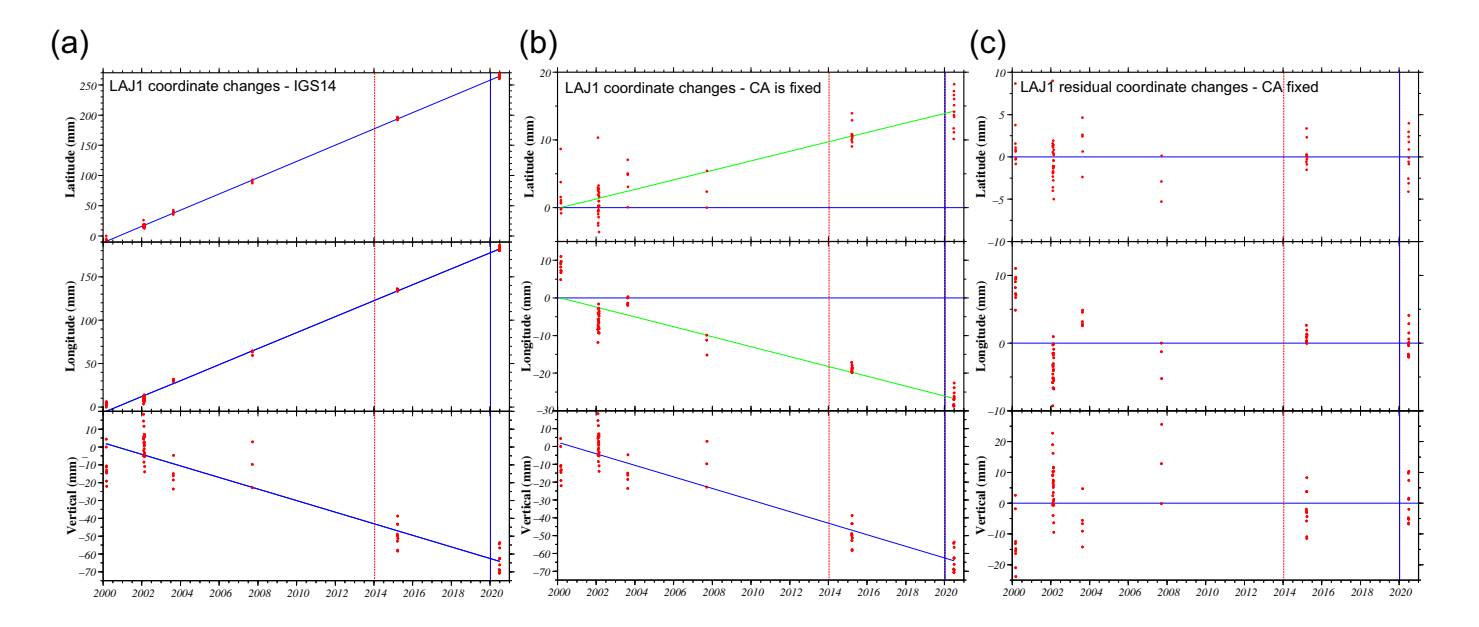


**Figure 5.** cGPS station PRLT in Cabo Rojo, Puerto Rico, in which method (2), a five-day offset was applied for the 7 January 2020 and 3 July 2020 earthquakes shown as vertical blue lines. Another regional earthquake occurred on 13 January 2014 is denoted with the dashed vertical red line,

although no offset was estimated. (a) The 24 hr position estimates relative to IGS14, (b) relative to the fixed-CA, and (c) with CA motion removed. Note the well-resolved afterslip in the north and east components. The color version of this figure is available only in the electronic edition.



unsurprising, particularly, because the suggested complex rupture process during this event may have yielded a deformation pattern arising from multiple contributing faults. We can, however, examine which sites agree with each of the nodal plane estimates. The preferred fault-plane solution, MNP1 (Cromwell et al., 2021; Vičič et al., 2021; ten Brink et al., 2022), dips to the north and strikes east-west. Although sites west of the epicenter are in overall good agreement with predictions, sites to the north fail to agree in both direction and magnitude. Site PRGY, immediately north of the epicenter, shows a larger than computed northeast displacement and a 90° misfit to the predicted coseismic displacement. Interestingly, campaign site CCM5 in Ponce agrees well with the predicted southwest displacement direction, albeit with a far larger displacement. Farther north, episodic site ADJN shows agreement in the direction but with a larger displacement, thus failing to produce a similar smaller magnitude to the prediction. Of sites west of the epicenter where a consistent northwest prediction is observed, an interesting result comes from the eGPS site LAJ1, where a large displacement is observed toward west-southwest. With respect to sites east of the epicenter, eGPS sites CAJA and SALN produce discrepant results. Site CAJA shows a displacement toward eastsoutheast, almost 180° from the prediction, and site SALN shows a larger displacement toward the north, where the prediction is almost negligible.

When the northeast–southwest-striking southeast-dipping nodal plane is used (MNP2), results from GPS observations at sites to the north of the epicenter tend to provide better agreement (Fig. 8). Site ADJN has the best-fit direction but has larger observed displacement, whereas both PRGY and CCM5 have smaller predicted displacement, with a direction similarly oriented to what was observed. GPS sites to the west, however, show smaller displacements when compared to the observed values. GPS sites located to the east of the epicenter produce disagreements in both orientation and magnitude of the

**Figure 6.** Campaign GPS station LAJ1 in San German, Puerto Rico, in which method (1), a constant velocity offset was applied for the 7 January 2020 earthquake, shown as vertical blue line. Another regional earthquake, which occurred on 13 January 2014, is denoted with the dashed vertical red line, although no offset was estimated. Panel (a) shows each 24 hr position estimate relative to IGS14, (b) relative to the fixed-CA, and (c) with CA motion removed. Note that because the previous occupation at LAJ1 was in 2015 and the most recent was several months after the 7 January 2020 earthquake, this is the only viable method to estimate the coseismic displacement. The color version of this figure is available only in the electronic edition.

predicted displacement. We note that the southwest-dipping fault plane favors a larger, westward displacement for CAJA than the prediction for the northwest-dipping nodal plane.

The comparison of our GPS-derived coseismic observations with the predicted displacements from the USGS NEIC focal mechanism's nodal planes confirm that irrespective of which nodal plane is used for the fault plane, the predicted static displacement computed at these sites fail to reproduce the observed values across the entire GPS network. A direct inversion of the GPS-derived coseismic displacements together with seismic data is necessary to compute a focal plane that would better explain the actual rupture process that occurred during the complex,  $M_{\rm w}$  6.4 event of 7 January 2020.

# The 3 July 2020 aftershock

GPS-derived coseismic observations for the 3 July 2020 aftershock indicate that deformation for this event is confined south of the fault, because displacements were observed only in cGPS sites PRMI, and SBPR, and eGPS site PARG. Recall that sites PRMI and PARG are located ~100 m apart. PRMI is a rooftop site installed in 2006, and PARG is a Bevis pin drilled into exposed rock in the 80's (Dixon *et al.*, 1998). PARG was occupied once after the mainshock and once again after the 3 July 2020 aftershock.

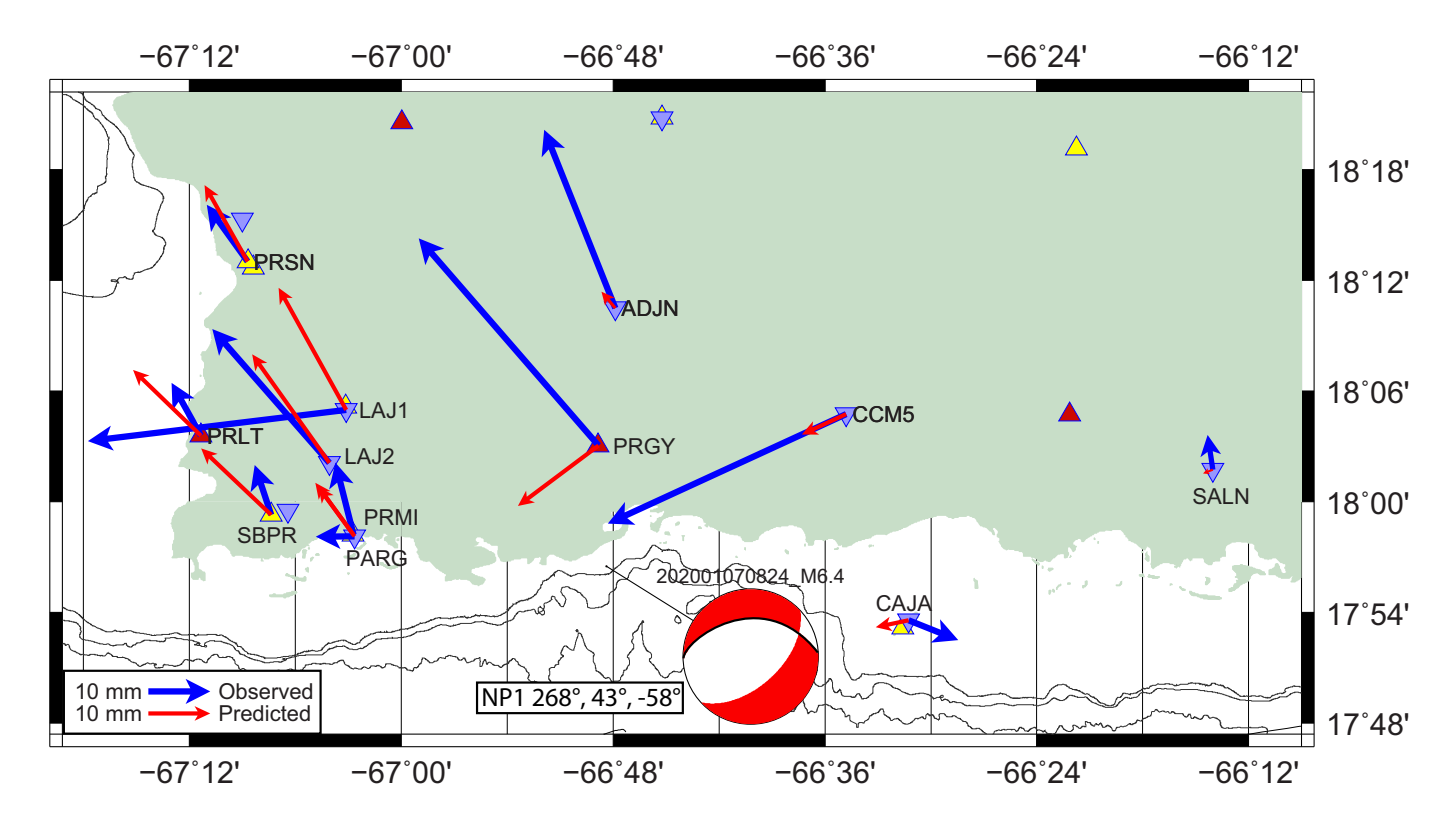


**Figure 7.** Observed (blue vectors) and predicted (red) coseismic displacements for campaign and cGPS sites for the 7 January 2020 mainshock using the northward-dipping nodal plane (MNP1). Triangles are cGPS

sites: PRSN (yellow), HLCM (red), and inverted blue triangles are eGPS sites. The color version of this figure is available only in the electronic edition.

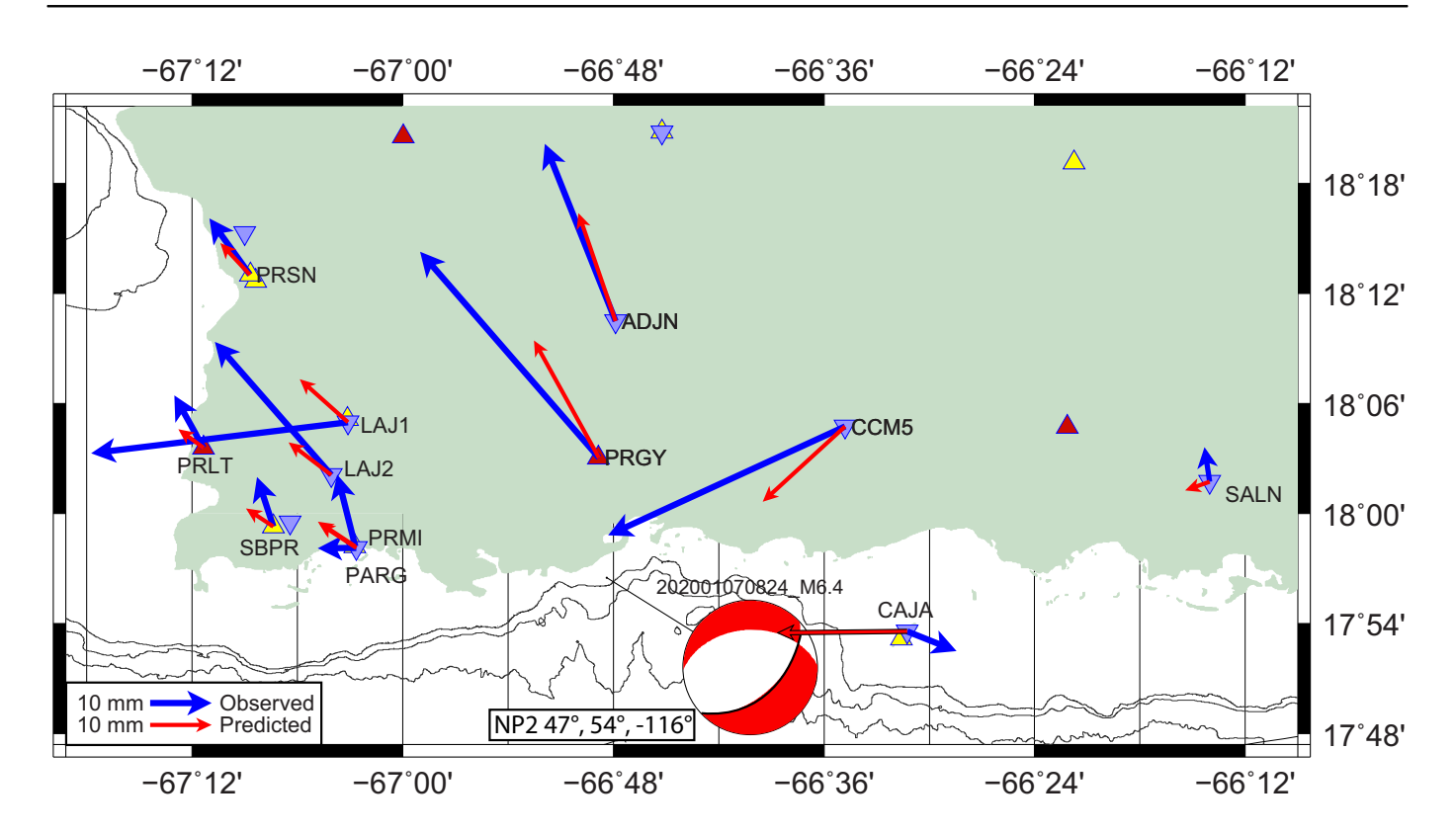


**Figure 8.** Observed (blue vectors) and predicted (red) coseismic displacements for campaign and cGPS sites for the 7 January 2020 mainshock using the southwest-dipping nodal plane (MNP2). Triangles are cGPS

sites: PRSN (yellow), HLCM (red), and inverted blue triangles are eGPS sites. The color version of this figure is available only in the electronic edition.

Volume 113 Number 1 February 2023 www.bssaonline.org

Bulletin of the Seismological Society of America • 10

TABLE 2 Displacement Comparisons (in Millimeters) for 7 January 2020  $M_{\rm w}$  6.4 Mainshock

	Observed Disp	placement (mm)		MNP1		MNP2		
Sites	N	E	U	N	E	N	E	
PRGY	33.418	-28.995	-8.503	-9.746	-13.011	19.027	-10.529	
PRMI	11.641	-2.933	-1.378	8.367	-6.151	3.995	-6.048	
PRLT	8.528	-4.741	0.458	10.575	-10.921	3.001	-4.056	
PRSN	9.116	-6.563	1.521	12.292	-6.929	5.13	-4.793	
PRJC	18.109	-1.939	2.099	9.219	-2.165	7.5	-4.155	
PRN4	-3.827	-3.93	6.982	-1.059	-2.795	-3.345	-7.331	
SBPR	8.053	-2.663	-7.318	10.748	-11.332	2.917	-4.418	
ADJN	28.763	-11.471	33.502	2.652	-2.234	17.542	-6.035	
CAJA	-3.200	8.015	-19.555	-1.125	-5.32	-0.24	-21.0	
CCM5	-17.691	-38.498	-19.664	-3.289	-7.128	-12.244	-13.385	
LAJ1	-5.042	-41.724	61.639	19.688	-10.899	7.005	-7.846	
LAJ2	21.591	-18.893	-9.805	17.512	-12.456	5.309	-6.963	
PARG	-0.058	-6.300	51.540	8.033	-5.849	3.971	-6.024	
SALN	-0.847	5.644	4.957	-0.614	-1.589	-1.412	-3.971	

MNP1 and MNP2 are predicted displacements for fault parameters using nodal planes 1 and 2, respectively. Sites in bold are continuous.

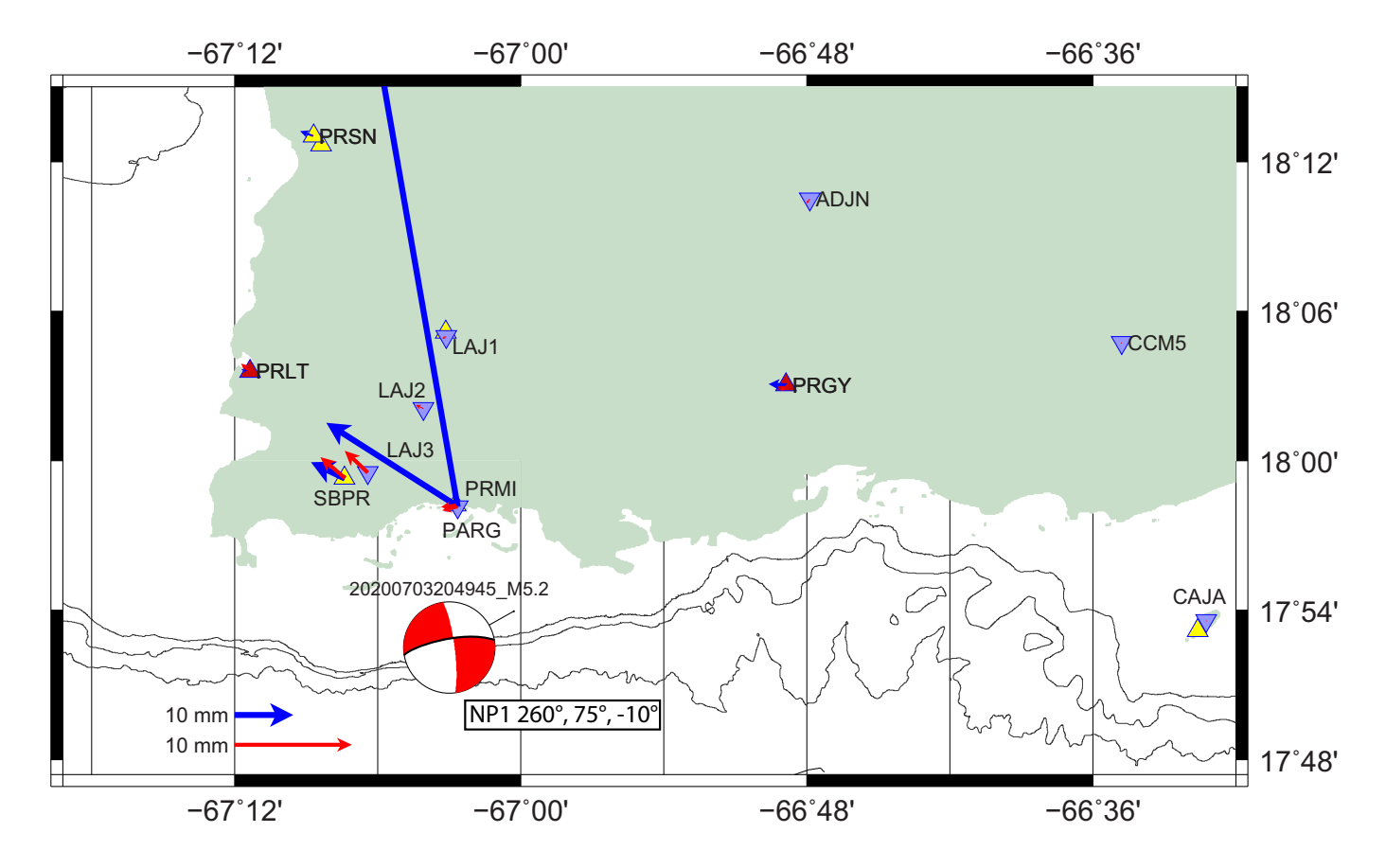
TABLE 3 Displacement Comparisons (in Millimeters) for 3 July 2020  $M_w$  5.3 Mainshock

Site	Observed Dis	splacement (mm)		ANP1		ANP2		
	N	E	U	N	E	N	E	
PRGY	0.116	-3.116	-1.321	-0.543	-0.52	-0.665	-0.658	
PRMI	14.082	-22.127	-3.376	-0.184	-1.3	3.603	-3.707	
PRLT	0.229	-1.534	-0.396	0.671	-0.776	0.654	-0.855	
PRSN	0.822	-2.239	-9.289	0.123	-0.18	0.195	-0.223	
PRJC	-0.208	-0.918	8.326	-0.106	-0.084	-0.092	-0.089	
PRN4	3.13	-2.328	2.709	-0.047	-0.018	-0.05	-0.017	
SBPR	2.802	-5.802	-10.742	1.789	-2.09	1.511	-2.319	
PARG	88.436	-15.438	-60.888	-0.296	-1.31	3.648	-3.767	

ANP1 and ANP2 are predicted displacements for fault parameters using nodal planes 1 and 2, respectively. Sites in bold are continuous.

Because the southwestern Puerto Rico region has a characteristic west-northwest-east-southeast-trending left-lateral strike-slip system (Huérfano et al., 2004), it was natural to select the left-lateral fault plane from the first focal mechanisms in the seismic sequence. In addition, the fact that the identified onland fault in the region (PMF) has a similar trend, and motion to those focal mechanisms was an important decision factor in establishing a relationship between the events and a possible offshore extension of the PMF early on in the seismic sequence. However, the fact that the 3 July 2020 aftershock occurred farther south than the trend of the PMF could mean that either another similarly trending left-lateral fault exists offshore, or that a northeast-southwest-trending right-lateral fault is accommodating deformation. To test this idea, we computed static displacements using both the nodal faults and compared to observed displacements at sites PRMI, SBPR, and PARG.

Figure 9 and Table 3 show displacement comparisons between observed and predictions using the east-west-trending left-lateral fault-plane solution (ANP1), whereas Figure 10 shows comparisons using the right-lateral north-south-trending fault solution (ANP2). It is evident that ANP2, the northsouth-trending fault plane, produces better agreement at site PRMI and an excellent fit at SBPR, suggesting that the 3 July 2020 aftershock may have occurred along a northsouth-trending right-lateral strike-slip fault as previously suggested by ten Brink et al. (2022) and unlikely associated to a left-lateral fault parallel to PMF as initially suggested by López-Venegas, Hughes, and Vanacore (2020). The observed horizontal displacements at PRMI for this event were larger than those observed during the mainshock (14.082 mm vs. 11.641 mm and -22.127 mm vs. -2.933 mm for the north and east components, respectively). Both PRMI and PARG were the closest sites to the epicenter for the 3 July 2020



 $M_{\rm w}$  5.3 aftershock, and no other site experienced the same behavior. An unexpectedly high displacement at PARG was observed between the occupation after the mainshock and the occupation immediately after the 3 July 2020 aftershock.

# Postseismic velocity field

A preliminary analysis of cGPS data after the 3 July 2020 aftershock for existing sites and for the six RAPID sites is shown in Figure 11. The data cutoff date is until 20 November 2021, and it shows no apparent velocity pattern in the region, owing to its current reaccommodation process prior to the beginning of the next interseismic period. Sites that appear to be south of the PMF, however, show faster velocities; SBPR, LVFP, MBGP. Whether this is an artifact of the short time span of these sites or if it is truly showing faster movement of the SWPR block will require additional data and analysis.

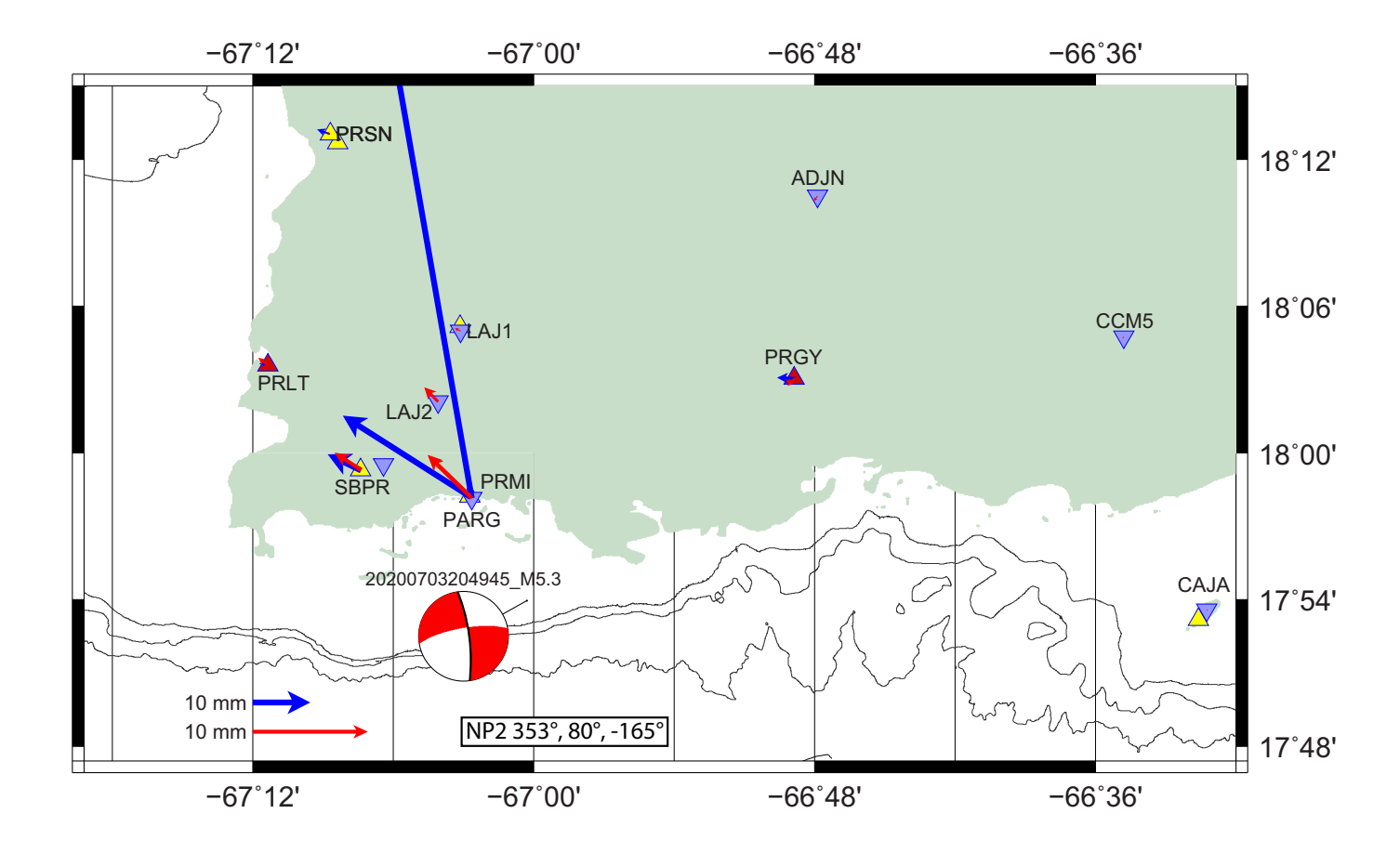
#### CONCLUSION

The 7 January 2020  $M_{\rm w}$  6.4 Southwest Puerto Rico earthquake was triggered by a left-lateral foreshock sequence, and it was followed by a complex rupture process along multiple transtensional faults. The subduction of the NA plate beneath the CA plate in a northeast–southwest oblique direction causes localized deformation along the PRVI block and its boundaries. Active and slow transtensional tectonic deformation throughout the Mona Passage is diffuse with a plausible albeit

**Figure 9.** Observed (blue vectors) and predicted (red) coseismic displacements for campaign and cGPS sites for the 3 July 2020 aftershock using the steeply northward-dipping left-lateral nodal plane (ANP1). Only the campaign site PARG, and cGPS sites PRMI and SBPR recorded postseismic displacements associated with this aftershock. The color version of this figure is available only in the electronic edition.

uncertain relationship with the 2020 southwest PR seismic sequence farther southeast.

The USGS-derived focal mechanism of the 7 January mainshock and 3 July aftershock were used to determine static displacements at GPS sites. GPS data from continuous and episodic sites in southwestern PR were used to estimate and discriminate among the nodal planes of the USGS. Our study is in agreement with other studies in that we infer that the northwestward-dipping nodal plane as the predominant causative fault for the mainshock. Some disagreements still exist between the observed and predicted displacements, however, and this suggests that a complex faulting mechanism for the 7 January 2020 mainshock occurred, as previously suggested (Liu et al., 2020; Cromwell et al., 2021; Blasweiler et al., 2022), and indicates that the southwestern PR region is a young deformation zone (Viltres et al., 2021; ten Brink et al., 2022). Postearthquake deployment of six continuous GNSS sites installed to monitor the onland PMF, west of the epicentral region, shows effects of



postearthquake afterslip, and additional data are expected to provide valuable insights into the possible loading of inland faults after the 2020 earthquake sequence.

#### **DATA AND RESOURCES**

Hatanaka-compressed Global Positioning System (GPS) data in RINEX 2.11 format from continuous stations were acquired from two primary archives including UNAVCO (https://data.unavco.org/archive/gnss/) and the National Geodetic Survey (NGS) Continuous Operating Reference Station (CORS) network (https://geodesy.noaa.gov/corsdata/ rinex/). Final, nonfiducial orbit, clock, and Earth orientation (OEP) products (Repro3-IGS14-Lichten and Border (see 1987) were obtained from the Jet Propulsion Laboratory (JPL) (https:// sideshow.jpl.nasa.gov/pub/JPL\_GPS\_Products/Final/). This study is in IGS14 (Altamimi et al., 2016, https://www.iers.org/IERS/EN/ DataProducts/ITRF/itrf.html). Ocean loading coefficients corrected for both ocean and solid earth motion, and using the FES2004 global gravity model were obtained from the Onsala Space Observatory (http:// holt.oso.chalmers.se/loading/). Tropospheric delays were estimated using standard VMF1 2.5 × 2 grid (Boehm et al., 2006) files from the Technical University of Vienna (https://vmf.geo.tuwien.ac.at). Maps and graphs were produced using the Generic Mapping Tools (GMT) software (Wessel and Smith, 1998, https://www.generic-mapping-tools.org/). All websites were last accessed in March 2022.

#### **DECLARATION OF COMPETING INTERESTS**

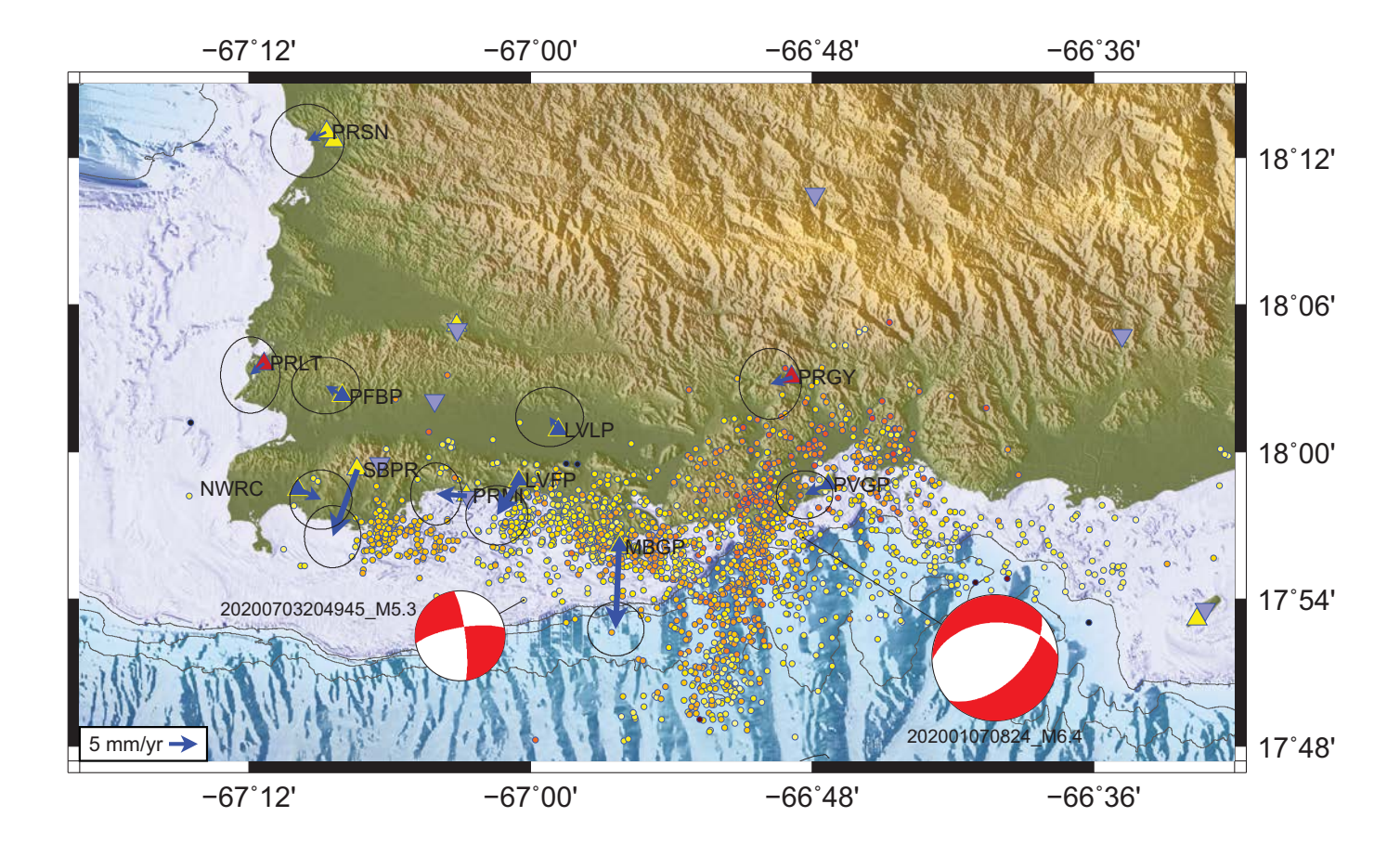
The authors acknowledge that there are no conflicts of interest recorded.

**Figure 10.** Observed (blue vectors) and predicted (red) coseismic displacements for campaign and cGPS sites for the 3 July 2020 aftershock using the steeply east-dipping right-lateral nodal plane (ANP2). The color version of this figure is available only in the electronic edition.

#### **ACKNOWLEDGMENTS**

The authors would like to thank the Puerto Rico Seismic Network (PRSN) for providing logistical help in the occupation of campaign sites immediately after the mainshock. Alberto M. López-Venegas appreciates the help of UPRM Department of Geology undergraduate students Zujeylees López and Armaris Rosado for occupation of campaign sites during 2021. Alberto M. López-Venegas wishes to thank UNAVCO for all assistance and equipment loan for the RAPID deployment, in particular, to Jim Normandeau and Keith Williams. The authors acknowledge HLCM Group for providing free access to Global Positioning System (GPS) data from their sites through the National Geodetic Survey (NGS) Continuous Operating Reference Station (CORS) program. Part of this work was funded by the NSF-EAR RAPID Award Number 2022264. David J. Mencin and Glen S. Mattioli were funded by the Enabling Discoveries in Multiscale Earth System Dynamics: Geodetic Facility for the Advancement of Geoscience (GAGE) Cooperative Agreement (NSF-1724794). The authors appreciate useful reviews from anonymous reviewers in helping this article become a valuable contribution.

• Bulletin of the Seismological Society of America



#### **REFERENCES**

Addarich-Martínez, L. (2009). The geologic mapping and history of the Guánica quadrangle, southwestern Puerto Rico, Unpublished *Master's Thesis*, University of Puerto Rico, Mayagüez, Puerto Rico.

Altamimi, Z., P. Rebischung, L. Métivier, and X. Collilieux (2016). Itrf2014: A new release of the international terrestrial reference frame modeling nonlinear station motions, *J. Geophys. Res.* **121**, no. 8, 6109–6131, doi: 10.1002/2016JB013098.

Benford, B., C. DeMets, and E. Calais (2012). GPS estimates of microplate motions, northern Caribbean: Evidence for a Hispaniola microplate and implications for earthquake hazard, *Geophys. J. Int.* 191, no. 2, 481–490, doi: 10.1111/j.1365-246X.2012.05662.x.

Blasweiler, M., M. W. Herman, F. Houtsma, and R. Govers (2022). Tectonic context and possible triggering of the 2019–2020 Puerto Rico earthquake sequence, *Seismol. Res. Lett.* **93**, no. 2A, 584–593, doi: 10.1785/0220210224.

Boehm, J., B. Werl, and H. Schuh (2006). Troposphere mapping functions for GPS and very long baseline interferometry from European centre for medium range weather forecasts operational analysis data, *J. Geophys. Res.* 111, no. B2, doi: 10.1029/2005JB003629.

Chaytor, J., and U. S. ten Brink (2010). Extension in Mona Passage, Northeast Caribbean, *Tectonophysics* **493**, 74–92, doi: 10.1016/j.tecto.2010.07.002.

Cromwell, C. W., K. P. Furlong, E. A. Bergman, H. M. Benz, W. L. Yeck, and M. Herman (2021). Seismotectonic analysis of the 2019–2020 Puerto Rico sequence: The value of absolute earthquake relocations in improved interpretations of active tectonics, *Seismol. Res. Lett.* **93**, no. 2A, 544–554, doi: 10.1785/0220210238.

**Figure 11.** Postearthquake velocity field derived from all southwestern PR cGPS sites, including the National Science Foundation Rapid Response Research (NSF RAPID) 2021 deployment.

DeMets, C., R. G. Gordon, and D. F. Argus (2010). Geologically current plate motions, *Geophys. J. Int.* **181**, 1–80.

DeMets, C., P. Jansma, G. S. Mattioli, T. H. Dixon, F. Farina, R. Bilham, E. Calais, and P. Mann (2000). GPS geodetic constraints on Caribbean-North America plate motion, *Geophys. Res. Lett.* 27, 437–440.

DeMets, C., G. Mattioli, P. Jansma, R. Rogers, C. Tenorio, and H. L.
 Turner (2007). Present motion and deformation of the Caribbean
 Plate in Northern Central America, in Geologic and Tectonic
 Development of the Caribbean Plate in Northern Central
 America, P. Mann (Editor), The Geological Society of America,
 Boulder, Colorado, 1–36.

Dixon, T. H., F. Farina, C. DeMets, P. Jansma, P. Mann, and E. Calais (1998). Relative motion of the Caribbean plate and associated boundary zone deformation based on a decade of GPS observations, *J. Geophys. Res.* **103**, 15,157–15,182.

Doser, D. I., C. M. Rodríguez, and C. Flores (2005). Historical earthquakes of the Puerto Rico-Virgin Islands region (1915-1963), in Active Tectonics and Seismic Hazards of Puerto Rico, the Virgin Islands, and Offshore Areas, P. Mann (Editor), The Geological Society of America, Boulder, Colorado, 103–114.

Granja Bruña, J. L., U. S. ten Brink, A. Martín Muñoz, A. Carbó-Gorosabel, P. Llanes, and Estrada (2015). Shallower structure

- and geomorphology of the southern Puerto Rico offshore margin, *Mar. Pet. Geol.* **67**, 30–56, doi: 10.1016/j.marpetgeo.2015.04.014.
- Heflin, M., W. Bertiger, G. Blewitt, A. Freedman, K. Hurst, S. Lichten, U. Lindqwister, Y. Vigue, F. Webb, T. Yunck, et al. (1992). Global geodesy using GPS without fiducial sites, Geophys. Res. Lett. 19, 131–134.
- Huérfano, V., C. von-AndradeHillebrandt, and G. Báez-Sánchez (2004).
  Microseismic activity reveals two stress regimes in southwestern Puerto Rico, in Active Tectonics and Seismic Hazards of Puerto Rico, the Virgin Islands, and Offshore Areas, P. Mann (Editor), The Geological Society of America, Boulder, Colorado, 1–61.
- Ihemedu, D. (2012). An updated GPS velocity field for Puerto Rico and the Virgin Islands: Constraints on tectonic setting and internal-deformation, *Unpublished Master's Thesis*, University of Texas, Arlington, Texas.
- Jansma, P. E., and G. M. Mattioli (2005). GPS results from Puerto Rico and the Virgin Islands: Constraints on tectonic setting and rates of active faulting, in P. Mann (Editor), Special paper 385, The Geological Society of America, Boulder, Colorado, 13–30.
- Jansma, P. E., G. M. Mattioli, A. M. López, C. D. DeMets, T. H. Dixon, P. Mann, and E. Calais (2000). Neotectonics of Puerto Rico and the Virgin Islands, northeastern Caribbean, from GPS geodesy, *Tectonics* 19, no. 6, 1021–1037.
- Laurencin, M., B. Marcaillou, D. Graindorge, F. Klingelhoefer, S. Lallemand, M. Laigle, and J.-F. Lebrun (2017). The polyphased tectonic evolution of the Anegada passage in the northern lesser Antilles subduction zone, *Tectonics* 36, no. 5, 945–961, doi: 10.1002/2017TC004511.
- Lichten, S. M. (1990). Estimation and filtering for high-precision GPS positioning applications, *Manuscr. Geod.* **15**, 159–176.
- Lichten, S. M., and J. S. Border (1987). Strategies for high-precision global positioning system orbit determination, *J. Geophys. Res.* **92**, no. B12, 12,751–12,762, doi: 10.1029/JB092iB12p12751.
- Liu, C., T. Lay, Z. Wang, and X. Xiong (2020). Rupture process of the 7 January 2020, Mw 6.4 Puerto Rico earthquake, *Geophys. Res. Lett.* 47, no. 12, e2020GL087718, doi: 10.1029/2020GL087718.
- López, A. M., P. E. Jansma, G. S. Mattioli, S. A. James, D. Ihemedu, S. M. Quintana, and J. S. Salazar (2011). Constraining Puerto Rico—Virgin Islands microplate internal deformation with two decades of GPS observations, AGU Fall Meeting Abstracts, Abstract T23D-2450 Presented at Fall 2011 Meeting, AGU, San Francisco, California, 7 December.
- López-Venegas, A., S. Hughes, and E. Vanacore (2020). Puerto Rico's Winter 2019–2020 seismic sequence leaves the island on edge, *Temblor.net*, doi: 10.32858/temblor.064.
- López-Venegas, A., S. Hughes, E. Vanacore, G. Báez-Sánchez, and T. Hudgins (2020). Response and initial scientific findings from the southwestern Puerto Rico 2020 seismic sequence, *Temblor.net*, doi: 10.32858/temblor.068.
- Mann, P., and K. Burke (1984). Neotectonics of the Caribbean, *Rev. Geophys.* **22**, no. 4, 309–362.

- Mao, A., C. Harrison, and T. Dixon (1999). Noise in GPS time series, *J. Geophys. Res.* **104**, 2797–2816.
- Masson, D. G., and K. M. Scanlon (1991). The neotectonic setting of Puerto Rico, *Geol. Soc. Am.* **103**, 144–154.
- Reasenberg, P., and L. M. Jones (1989). Earthquake hazard after a mainshock in California, Science 243, no. 4895, 1173–1176.
- Roig-Silva, C. M., E. Asencio, and J. Joyce (2013). The Northwest trending North Boquerón Bay-Punta Montalva fault zone; a through going active fault system in southwestern Puerto Rico, Seismol. Res. Lett. 84, no. 3, 538–550.
- Scherneck, H.-G. (1991). A parametrized solid earth tide model and ocean tide loading effects for global geodetic baseline measurements, *Geophys. J. Int.* **106**, no. 3, 677–694.
- Solares-Colón, M. (2019). New constraints on crustal deformation within the Puerto Rico-Virgin islands microplate using two decades of GPS data, *Unpublished Master's Thesis*, University of Puerto Rico, Mayagüez, Puerto Rico.
- ten Brink, U., E. Vanacore, E. Fielding, J. Chaytor, A. López-Venegas, W. Baldwin, D. S. Foster, and B. Andrews (2022). Mature diffuse tectonic block boundary revealed by the 2020 southwestern Puerto Rico seismic sequence, *Tectonics* **41**, no. 3, e2021TC006896, doi: 10.1029/2021TC006896.
- ten Brink, U. S., S. Marshak, and J.-L. G. Bruña (2009). Bivergent thrust wedges surrounding oceanic island arcs: Insight from observations and sandbox models of the northeastern Caribbean plate, *GSA Bull.* **121**, nos. 11/12, 1522–1536.
- van der Elst, N. J., J. L. Hardebeck, A. J. Michael, S. K. McBride, and E. Vanacore (2022). Prospective and retrospective evaluation of the U.S. Geological Survey Public aftershock forecast for the 2019–2021 Southwest Puerto Rico Earthquake and aftershocks, *Seismol. Res. Lett.* **93**, no. 2A, 620–640.
- Vičič, B., S. Momeni, A. Borghi, A. Lomax, and A. Aoudia (2021). The 2019–2020 southwest Puerto Rico earthquake sequence: Seismicity and faulting, *Seismol. Res. Lett.* **93,** no. 2A, 533–543, doi: 10.1785/0220210113.
- Viltres, R., A. Nobile, H. Vasyura-Bathke, D. Trippanera, W. Xu, and S. Jónsson (2021). Transtensional rupture within a diffuse plate boundary zone during the 2020 Mw 6.4 Puerto Rico earthquake, *Seismol. Res. Lett.* **93**, no. 2A, 567–583, doi: 10.1785/0220210261.
- Wessel, P., and W. H. F. Smith (1998). New, improved version of generic mapping tools released, *Eos Trans. AGU* **79**, no. 47, 579–579, doi: 10.1029/98EO00426.
- Zumberge, J. F., M. Heflin, D. Jefferson, M. Watkins, and F. Webb (1997). Precise point positioning for efficient and robust analysis of GPS data, *J. Geophys. Res.* **102**, 5005–5018.

Manuscript received 21 June 2022 Published online 16 December 2022